

1 Intermittent turbulence, noisy fluctuations and wavy
2 structures in the Venusian magnetosheath and wake

Z. Vörös,¹ T. L. Zhang,² M. P. Leubner,¹ M. Volwerk,² M. Delva,² and W.
Baumjohann,²

arXiv:0901.1570v1 [astro-ph.EP] 12 Jan 2009

Z. Vörös, Institute of Astro- and Particle Physics, University of Innsbruck, Technikerstr. 25,
6020 Innsbruck, Austria. (zoltan.voeroes@uibk.ac.at)

¹Institute of Astro- and Particle Physics,
University of Innsbruck, Innsbruck, Austria.

²Space Research Institute, Austrian
Academy of Sciences, Graz, Austria.

3 **Abstract.** Recent research has shown that distinct physical regions in
4 the Venusian induced magnetosphere are recognizable from the variations
5 of strength of the magnetic field and its wave/fluctuation activity. In this pa-
6 per the statistical properties of magnetic fluctuations are investigated in the
7 Venusian magnetosheath and wake regions. The main goal is to identify the
8 characteristic scaling features of fluctuations along Venus Express (VEX) tra-
9 jectory and to understand the specific circumstances of the occurrence of dif-
10 ferent types of scalings. For the latter task we also use the results of mea-
11 surements from the previous missions to Venus. Our main result is that the
12 changing character of physical interactions between the solar wind and the
13 planetary obstacle is leading to different types of spectral scaling in the near-
14 Venusian space. Noisy fluctuations are observed in the magnetosheath, wavy
15 structures near the terminator and in the nightside near-planet wake. Multi-
16 scale turbulence is observed at the magnetosheath boundary layer and near
17 the quasi-parallel bow shock. Magnetosheath boundary layer turbulence is
18 associated with an average magnetic field which is nearly aligned with the
19 Sun-Venus line. Noisy magnetic fluctuations are well described with the Gaus-
20 sian statistics. Both magnetosheath boundary layer and near shock turbu-
21 lence statistics exhibit non-Gaussian features and intermittency over small
22 spatio-temporal scales. The occurrence of turbulence near magnetosheath
23 boundaries can be responsible for the local heating of plasma observed by
24 previous missions.

1. Introduction

25 The structured plasma environment of Venus is a natural plasma laboratory where the
26 planetary ionosphere acts as an obstacle to the supersonic solar wind flow carrying a mag-
27 netic field. The absence of an intrinsic magnetic field ensures that this interaction is more
28 comet-like than Earth-like. It is known from the previous missions to Venus (e.g., Russell
29 and Vaisberg, 1983) that the most prominent features include the direct interaction of
30 ionized magnetosheath flow with the ionosphere/quasi-neutral atmosphere, mass loading
31 of the magnetosheath flux-tubes, and the transport/convection of magnetic flux to the
32 wake region, representing also the dominant source for the magnetotail fluxes. However,
33 for most of the time, mainly during time intervals of low solar wind dynamic pressure,
34 the induced and piled up magnetic field around the planetary obstacle represents an ef-
35 fective magnetic barrier, preventing free entrance of solar wind plasma to the Venusian
36 ionosphere (Zhang et al., 2007). The draping of the interplanetary magnetic field (IMF),
37 the accretion of magnetic flux by the planet, the characteristic spatial scales of physical
38 processes as well as the location and specific features of boundaries, all depend on dynam-
39 ical processes in the solar wind and make this environment unique. The results of Venus
40 Express spacecraft (VEX) provide an altitude for the induced magnetopause of about 300
41 km at the subsolar point, while the subsolar bow shock distance from the surface of the
42 planet is about 1900 km (Zhang et al., 2007). These values exhibit a solar cycle depen-
43 dence, i.e. the thickness of the Venusian magnetosheath varies around 1500 km at the
44 subsolar point and widens up to 5000 - 7000 km at the terminator. During time intervals
45 of high solar wind dynamic pressure, the ionopause moves to low altitude (~ 250 km) and

46 mainly the ionosphere forms the obstacle responsible for deflecting the solar wind flow.
47 In this case the thickness of the ionopause increases and more direct interaction between
48 the ionosphere and solar wind is possible (Elphic et al., 1981; Russel and Vaisberg, 1983).

49 In the dayside magnetosheath strong magnetic fluctuations and waves are present (e.g.
50 Luhmann et al., 1983). Mirror mode waves were observed here in case studies (Volwerk
51 et al., 2008a), and also investigated statistically (Volwerk et al., 2008b). On the other
52 hand, the limited spatial scale of the magnetosheath on the dayside might not support a
53 development of a turbulent cascade, the fluctuations rather resemble $1/f$ noise (f is the
54 frequency). $1/f^\alpha$ noise is a signature of the presence of independent physical mechanisms
55 driving fluctuations in the magnetosheath (Vörös et al., 2008). Keeping in mind that the
56 ion inertial length is of the order of 100 km, the magnetohydrodynamic (MHD) spatial
57 scales in the Venusian magnetosheath are limited to one or two decades in wave-number
58 space.

59 The terminator and, further downstream, the night-side region is of particular interest
60 (Spreiter and Stahara, 1992). Here plasma instabilities, vortices, and turbulence can
61 develop near boundaries. For example, Wolff et al. (1980) have shown that the distortion
62 of the ionopause by Kelvin-Helmholtz instability might lead to the formation of magnetic
63 flux ropes inside the ionosphere as well as ionospheric bubbles embedded in the solar
64 wind. Numerical simulations indicate that the Kelvin-Helmholtz instability can occur
65 at the terminator ionopause of Venus (Terada et al., 2002), capable of producing wave
66 structures over 1000 km in size (Amerstorfer et al., 2007; Biernat et al., 2007). In fact, the
67 initial VEX observation detected these wavy structures (Balikhin et al., 2008). A recent
68 study shows that MHD turbulence near and immediately after the terminator is not

69 fully developed because of the rapid decrease of spectral power toward higher frequencies,
70 resulting in spectral scaling indices $\alpha > 2$ (Vörös et al., 2008). Further downstream,
71 in the magnetotail/magnetosheath region, the spectral analysis indicates the presence of
72 developed inertial range turbulence, with a spectral scaling index $\alpha \sim 1.6$, close to the
73 values expected for hydrodynamic or magnetohydrodynamic turbulent flows. However,
74 in the same region, non-gaussian probability density functions (PDF) with typical long
75 tails, corresponding to intermittent turbulence, were not observed (Vörös et al., 2008).
76 This can be explained by the shortness of turbulent time series during a tail-crossing, in
77 particular not allowing a full reconstruction of PDF tails.

78 The near-Venus tail is highly structured. There is no significant plasma inflow into the
79 near-Venusian wake. The wake magnetic field is known to be stronger than the IMF and
80 from the cavity hot plasma is excluded (Bauer et al., 1977). The solar wind-ionosphere
81 interaction in the presence of the draped interplanetary magnetic field, however, produces
82 an extended boundary tailward from the terminator, at the inner edge of the magne-
83 topause, or outer edge of the wake downstream, where boundary layer turbulence can
84 develop and heat locally the plasma. The width of this boundary layer is limited, does
85 not include the whole plasma sheet. In order to understand the energy content and en-
86 ergy dissipation of underlying processes, it is necessary to investigate systematically the
87 statistical features of fluctuations in the structured near -Venusian plasma environment.
88 In this paper we statistically analyze the spectral scaling features of fluctuations in the
89 magnetosheath, wake and near -boundary regions using VEX magnetometer data during
90 the first twenty days in May 2006. The time resolution of the magnetic data is 1 s. Due
91 to rapid crossing of different structures, this time resolution is necessary for obtaining

92 statistically reliable scaling results. The main emphasis is on the analysis of scalings,
93 i.e. on the evaluation of the continuous part of magnetic power spectra. The analysis of
94 waves (when the continuous parts of the spectra are not considered) is equally important,
95 but out of the scope of this paper. In addition to spectral estimations, we will compare
96 the probability distribution functions (PDFs) and evaluate the scale dependency of their
97 shapes, associated with noisy and turbulent fluctuations. This helps to obtain a more
98 reliable differentiation between turbulence and noise, occurring along the VEX trajectory.
99 The near-polar orbit of VEX with a periapsis altitude of 250-350 km allows for the first
100 time observations at terminator and mid-magnetotail regions (Zhang et al., 2006). These
101 two important regions were not covered by the previous missions, e.g. Pioneer Venus
102 Orbiter (PVO, Russell, 1992).

2. Near-Venus plasma regions with varying spectral scaling properties

103 It was reported by Vörös et al. (2008) that the value of spectral scaling index α ,
104 describing the self-similarity of the power spectrum of the magnetic field data in the
105 frequency range 0.03 - 0.5 Hz, exhibits different values in different regions near Venus.
106 The magnetic fluctuations are non-stationary, e.g. in the magnetosheath the magnetic
107 field strength is increasing towards the induced magnetopause, which introduces a trend
108 into magnetic field data. In order to estimate α robustly, we used a wavelet method
109 proposed by Abry et al. (2000) and applied it successfully to the description of magnetic
110 fluctuations in the Earth's plasma sheet (Vörös et al., 2004). In this paper we use the
111 Daubechies wavelets, for which finite data size effects are minimized and the number of
112 vanishing moments can be changed. The latter feature of Daubechies analyzing wavelets

113 is essential to cancel the influence of polynomial trends or periodic structures in the data
114 on the estimation of the scaling index.

115 Let us demonstrate first how the spectral scaling features vary along the VEX trajectory
116 during its journey from the dayside magnetosheath through the terminator region and
117 wake to the post-terminator magnetosheath. As an example, we show the variation of total
118 magnetic field strength B on May 19, 2006 (Figure 1 top) together with the corresponding
119 power spectral densities (PSD) calculated during equally long time intervals (**a**, **b**, **c**, **d**
120 and **e**, Figure 1, bottom subplots) along the spacecraft trajectory. Zhang et al. (2007)
121 have already demonstrated that a crossing of each physical region in the near-Venus
122 plasma environment is recognizable from the variations of strength and wave/fluctuation
123 activity of the magnetic field. Indeed, B is not disturbed before $t_1 = 0115$ UT and after
124 $t_2 = 0310$ UT, the spacecraft is in the solar wind (Figure 1). The planetary obstacle
125 perturbs the magnetic field only between t_1 and t_2 . During the interval **a** VEX enters
126 the dayside magnetosheath from the solar wind (VEX trajectories and the intervals **a-e**
127 are shown in Figure 2, left bottom subplot). Here the magnetic field strength is strongly
128 fluctuating and its value increases up to ~ 50 nT. The estimated spectral scaling index
129 $\alpha = 1 \pm 0.2$ (the first bottom subplot in Figure 1) is low, indicating that fully developed
130 turbulence is absent in this region (Vörös et al., 2008). Higher values $\alpha = 5/3$ or $3/2$
131 are expected for hydrodynamic or MHD inertial range turbulence, respectively. After
132 ~ 0135 UT B decreases, which corresponds to the closest approach to Venus, VEX is
133 close to or below the induced magnetopause (Zhang et al. 2007). Between 0140 and
134 0205 UT high frequency fluctuations are absent, only low frequency wavy fluctuations are
135 seen. These wavy structures might be associated with Kelvin-Helmholtz instability at the

136 terminator ionopause or detached plasma clouds near the terminator, observed already
137 during Pioneer Venus orbits (Brace et al., 1982). During interval **b** the corresponding
138 spectrum exhibits significant wave power only near 0.07 Hz (~ 14 s) then the spectral
139 power rapidly decreases with a scaling index $\alpha = 2.5 \pm 0.2$ (the second bottom subplot in
140 Figure 1). Further downstream (after 0205 UT in Figure 1) broad-band fluctuations occur
141 again. The spectral indices within the intervals **c** and **e** are $\alpha = 1.5 \pm 0.2$ and 1.6 ± 0.2
142 respectively, indicating the presence of developed turbulence. In contrary, the interval **d**,
143 in between **c** and **e**, shows again $1/f$ noise-like scaling behavior (the last three bottom
144 subplots in Figure 1).

145 The physical difference between turbulence and noise is clear. Turbulence in the wake is
146 a consequence of nonlinear multi-scale interactions and it is strongly dissipative, heating
147 the background plasma at the small scales. Noisy fluctuations, exhibiting $1/f^\alpha$ scaling
148 behavior with α around 1, may have multiple physical sources not connected with nonlin-
149 ear interactions, typical for turbulence. $0 < \alpha < 1$ over higher frequencies (around 1Hz)
150 can also be associated with the noise of the magnetometer (Vörös et al., 2004). The low
151 values of α can also indicate that the spacecraft is not in a physical region where strong
152 nonlinear interactions and turbulence can exist, e.g., due to low plasma density or lack of
153 plasma flows. In the following, the notation '1/f noise' refers to $1/f^\alpha$ noise with spectral
154 scaling index in a range of $\alpha \in (0.6, 1.4)$ (find below the definition of the spectral index
155 used in this paper).

156 In this paper we put the emphasis on statistical examination of the circumstances
157 under which developed turbulence occurs in the post-terminator wake and magnetosheath
158 regions.

3. Statistical analysis of magnetic fluctuations

159 We investigated the time series of magnetic field strength statistically, obtained in the
160 near-Venusian space during the first twenty days in May 2006. During one day one orbit
161 is performed, therefore, during the twenty day interval we have observed twenty crossings.
162 Due to the non-homogeneity and dynamical nature of the near-Venus physical regions the
163 occurrence and the length of at least quasi-stationary intervals slightly differs each day.
164 We identified the approximate beginning and end of the steady intervals computing the
165 scaling indices over time scales 2-30 s, using the wavelet method within sliding overlapping
166 windows. After that, changing slightly the starting point and the length of turbulent/noisy
167 data, optimized data intervals with smallest errors in α were found. We rejected time
168 intervals where the error of the estimation of α was larger than ± 0.3 . The available
169 steady intervals in the dayside magnetosheath are shorter, so we selected 9 min long
170 intervals there. Further downstream 12 minute long intervals were selected. Selecting
171 longer data periods would significantly reduce the number of available intervals, while
172 shorter data sets would decrease the statistical reliability of results. Data intervals with
173 fluctuating magnetic field shorter than 12 minutes were not included into our analysis.
174 Due to occasional data gaps or shortness of steady fluctuations in the time series, the
175 number of events is not the same in different physical regions. There were crossings with
176 no steady fluctuations along the VEX trajectory. There were also crossings where the
177 time interval with steady fluctuations was longer than 24 minute.

178 Due to data gaps or shortness of statistically stationary time series, only 17 out of 20
179 crossings are shown in Figure 2 (left bottom and right subplots). A cylindrical coordinate
180 system is used in Figure 2, where the events are shown in $\sqrt{(Y^2 + Z^2)}$ VSO vs. X VSO

181 (bottom left) or in VSO coordinate pairs (right subplots). VSO is the Venus-centered
182 Venus-Sun-Orbital coordinate system, where X is in the direction of the Sun, Y opposite
183 to the orbital direction of Venus and Z perpendicular to the orbital plane, positive to
184 ecliptic north.

185 The near-Venusian space is physically non-homogeneous and the spatial and temporal
186 variations cannot be straightforwardly separated from single-spacecraft measurements.
187 Nevertheless, during the investigated time period in May 2006, the typical sequence of
188 physical regions visited by VEX remained approximately the same as in Figure 1: crossing
189 of the dayside magnetosheath (increasing B , interval **a**), low-frequency wavy structures
190 after the terminator (interval **b**) and entering into the region of broad-band fluctuations
191 further downstream (intervals **c-e**). The intervals **a-e** were introduced for the event on
192 May 19, 2006 (Figure 1: top and Figure 2: top-left). The wavy structures are not al-
193 ways present along the whole near-terminator region and wake. In the absence of the
194 wavy structures only low amplitude magnetometer noise is observed. Possibly, the occur-
195 rence/absence of wavy structures can be associated with the upstream conditions. For
196 example, during times when the solar wind dynamic pressure is high the ionopause moves
197 to low altitudes (~ 250 km), and direct interactions between the ionosphere and the solar
198 wind can occur (plasma-plasma interactions or solar wind electric field - ionospheric cur-
199 rents interactions). When the solar wind dynamic pressure is low the ionospheric width
200 increases (Elphic et al., 1981) and the draped IMF above ~ 300 km can stop the solar wind
201 more efficiently. In this paper we investigate only the features of magnetic fluctuations,
202 without considering the changes in the upstream conditions. The open triangles (Figure

203 2: bottom left) indicate the whole region (marks are only on the lowest trajectory) where
204 the wavy structures appear during the first 20 days in May 2006.

205 Due to the similarity of crossings, the depicted intervals (lines) along the trajectories
206 (Figure 2: bottom-left), in terms of spectral properties, refer generally to similar physical
207 regions along the VEX trajectory. For example, the thick black lines (Figure 2: bottom-
208 left) indicate turbulent processes identified through a spectral scaling index near $\alpha = 1.6$
209 . The location of turbulence in space approximately coincides with time intervals **c** and
210 **e**. The time interval **d** coincides roughly with the position of grey '+' signs along the
211 trajectory, where scaling indices corresponding to $1/f^\alpha$ noise were observed. For a better
212 visibility, the trajectories together with turbulent and noisy time intervals (**c**, **e** and **d**) are
213 depicted in the *VSO* coordinates (Figure 2: right subplots). From Figure 2 (right bottom)
214 it is visible that the spatial regions exhibiting the same α along multiple trajectories are
215 partially overlapping, indicating that these regions and the corresponding boundaries are
216 moving or the fluctuations are patchy or intermittent. Moving boundaries can appear in
217 connection with changing conditions in the solar wind.

218 Switching between temporal and spatial coordinates helps us to identify spatial regions
219 with typical scalings. Occasionally we will use plural indicating the change between
220 temporal and spatial coordinates. For example, the notation 'intervals **c**' means the set
221 of all crossings in space near the time interval/space region **c** on 19 May, 2006.

222 Figure 3 shows histograms with the number of events per unit interval of the scaling
223 index α , estimated during the time periods **a-e**. In each subplot, the horizontal lines over
224 the histograms represent the average of 95 % confidence limits for the mean in each value
225 of α . The largest average uncertainty corresponds to the dayside magnetosheath region,

226 where the length of analyzed data was shorter. Figure 3 indicates that the specific scaling
227 features characterize the statistical properties of different regions in space rather well.

228 During the magnetosheath periods (intervals **a** and **d**: top and bottom subplots in Fig-
229 ure 3) only two events display scaling indices > 1.3 , for the other events $\alpha \in (0.6 - 1.25)$.
230 This indicates that the fluctuations or waves present in the magnetosheath, except of a
231 few cases, usually do not evolve to a fully developed turbulence state. The observed range
232 of scaling indices suggests that the continuous part of the magnetosheath spectra is associ-
233 ated with $1/f$ noise rather than turbulence. Noisy fluctuations can be convected from the
234 dayside magnetosheath (interval **a**) to the post-terminator magnetosheath downstream
235 (interval **d**), where the spectral power is smaller, possibly the driving sources are more
236 distant than at the dayside (compare the spectra corresponding to the intervals **a** and **d**
237 in Figure 1).

238 In the post-terminator wake (intervals **b** in Figure 3) wavy structures dominate with
239 periods from 5 to 50 s (similar to event **b** in Figure 1). Since towards higher frequencies
240 the power rapidly decreases ($\alpha \sim 2.5$) independent driving sources associated with broad-
241 band noise or nonlinear multi-scale turbulence are absent.

242 Finally, a well discernible turbulence scaling index $\alpha \sim 1.6$ was observed during the
243 intervals **c** and **e** (Figure 3: third subplot from top). The events from both intervals are
244 plotted together because the corresponding scaling indices are similar.

245 The cartoon in Figure 4 helps to interpret the occurrence of typical scaling regimes,
246 summarizing the results of the statistical analysis along VEX trajectory in the cylindrical
247 VSO coordinate system: (1) $1/f$ noise appears under rather different conditions in the
248 magnetosheath: in front of the planetary obstacle and downstream in the post-terminator

249 magnetosheath (regions **a**, **d**: squares in Figure 4). Scaling indices which can be as-
250 sociated with turbulence occurred in $\sim 5\%$ of cases (see Figure 3); (2) Coherent wavy
251 fluctuations occur between the dayside magnetopause and post-terminator boundary of
252 the wake (largely within the optical shadow, region **b**: triangles in Figure 4), where noise
253 and turbulence are absent (only magnetometer noise is present when the wave activity
254 is absent). Closer to the terminator, the wavy structures can be associated with the
255 Kelvin-Helmholtz instability occurring at the terminator ionopause, resulting probably in
256 detached plasma clouds, first observed during the Pioneer Venus mission by Brace et al.
257 (1982). The PVO spacecraft observed filamentary structures (rays), density holes and
258 radially aligned draped magnetic field lines in the near-planet night side wake (Luhmann
259 and Russel, 1983; Marubashi et al., 1985); (3) Developed turbulence is present at or near
260 boundaries: at the wake/magnetopause/magnetosheath boundary and near the bow shock
261 (regions **c**, **e**: circles in Figure 4).

4. Discrimination between boundary turbulence and magnetosheath noise

262 Figure 3 shows that, in terms of spectral scaling characteristics, turbulence and noisy
263 intervals are well separable. In the following we will further investigate some other dif-
264 ferences between turbulence (intervals **c** and **e**) and noisy magnetosheath fluctuations
265 (intervals **d**). We first recall some similarities between the observations obtained from
266 previous missions and VEX near the regions with developed turbulence.

267 Early observations from Mariner 5 (Bridge et al., 1967) already showed the existence of
268 a plasma boundary located at the inner edge of the post-terminator magnetosheath (VEX
269 is crossing this region where the occurrence of turbulence is depicted by the bottom circle
270 in Figure 4). During a flyby, Mariner 5 found the location of the boundary layer from

271 ~ 3.2 to $4.5 R_V$ behind Venus and from ~ 2 (magnetopause location) to $3.5 R_V$ from the
272 center of the wake. Within the boundary layer Mariner 5 observed a strongly fluctuating
273 lower intensity magnetic field, a decrease of the density and velocity, but an increase of
274 the temperature. The magnetic field strength was larger when the spacecraft entered from
275 the inner magnetosheath, across the magnetopause, to the wake. VEX observations show
276 that the magnetopause location is rather variable over distances $XVSO < -1R_V$ (open
277 circles in Figure 2: left bottom). Therefore, multi-point turbulence fluctuations indicating
278 the crossing of the magnetopause start in different distances from the center of the wake.
279 For example, on May 19, 2006 (Figure 2: left top) the strongly fluctuating magnetic field
280 strength reaches a local maximum at about 0205 UT, then it slowly decreases. It indicates
281 that VEX is entering to the boundary layer from the wake (from intervals **b** to **c**) and
282 at the boundary the character of fluctuations is suddenly changing, from scaling index
283 $\alpha \sim 2.5$ to $\alpha \sim 1.6$ (see also Figure 1).

284 Another interesting feature includes the change of the sign of B_X . During the interval
285 **c** on May 19 it happens several times (Figure 2: top left). It can indicate that VEX is
286 crossing the neutral sheet behind the planet. The VEX trajectory for this day (marked
287 by an arrow in Figure 2, top right subplot) is roughly along $Y VSO \sim 0.9R_V$. In fact
288 the Venusian wake/magnetotail can be formed by flux tubes convected around or slipping
289 over the planet and filled with the plasma from the day side. At the same time, both
290 ends of the flux tubes are co-moving with the solar wind. In a simple case, the resulting
291 magnetic field in the tail is stretched along the X axis, because the central part of the
292 flux tubes is slowed down by the planet while both ends travel faster with the solar wind.
293 Since the IMF is usually close to the ecliptic plane, the tail current sheet, in ideal case,

294 should be formed by the stretched magnetic field mainly in the north-south plane (Russell
295 and Vaisberg, 1983). Depending on the upstream IMF and its draping around the planet,
296 the current sheet plane in the Venusian magnetotail can also rotate (Luhmann et al.,
297 1991). Since turbulence can drive local mixing and vorticity, the change of the magnetic
298 field direction might be also associated with turbulence, not necessarily with neutral sheet
299 crossing. For example, B_X is also changing sign several times during the shock associated
300 turbulence interval \mathbf{e} (Figure 2: top right), but it has nothing common with a neutral
301 sheet crossing.

302 The same magnetic field and plasma signatures of the inner magnetosheath boundary
303 layer were observed by other missions, too. For example, Venera 10 observed the bound-
304 ary layer tailward from the Mariner 5 flyby (Romanov et al., 1978). The near-terminator
305 part of the boundary layer was investigated during the Pioneer Venus Orbiter mission.
306 Perez-de-Tejada et al. (1991, 1993) have seen the boundary between the bow shock and
307 magnetopause (they are using the term ionopause instead) in the vicinity of and down-
308 stream from the terminator. The boundary layer observed in different distances along
309 the inner edge of magnetosheath confirms the persistent presence of this boundary as a
310 rarefaction wave emerging from the terminator magnetopause and extending downstream.
311 The high level of magnetic fluctuations and occurrence of magnetohydrodynamic waves
312 near a quasi-parallel Venusian bow shock is well-known from the PVO mission (Luhmann
313 et al., 1983). In this paper we emphasize the detection of intermittency near the Venu-
314 sian bow shock and its differentiation from magnetosheath noisy fluctuations. Also, we
315 investigate only the magnetic field signatures of the boundary layers.

4.1. Magnetic field orientation

316 First, we investigate the local magnetic conditions under which turbulence (or noise)
 317 can appear. For this purpose we calculate the instantaneous contribution of magnetic field
 318 VSO components to the total magnetic field: $b_X(t) = B_X(t)/B(t)$, $b_Y(t) = B_Y(t)/B(t)$
 319 and $b_Z(t) = B_Z(t)/B(t)$. In each time step t the sum $b_X^2(t) + b_Y^2(t) + b_Z^2(t) = 1$. Our goal
 320 is to compare the average magnetic field direction during turbulent (**c**, **e**) and noisy (**d**)
 321 intervals, when the scaling index is well defined (see Figure 2). Since α is a statistical
 322 descriptor over 12 min long intervals the mean values $\langle b_X^2 \rangle$, $\langle b_Y^2 \rangle$, and $\langle b_Z^2 \rangle$,
 323 respectively, were computed over the same time periods; their sum is again 1. Each
 324 average defines the relative contribution of a magnetic VSO component to the average
 325 magnetic strength during the considered intervals.

326 Figure 5 compares the local mean magnetic field components with the values of scaling
 327 indices estimated during the same 12 min long intervals (open and filled circles). The
 328 horizontal lines are averages of points over the noisy $\alpha < 1.4$ and turbulent $\alpha = 1.6 \pm 0.2$
 329 scaling index ranges. These distinct ranges of α correspond to the statistical results in
 330 Figure 3. The filled circles correspond to turbulent intervals within the magnetosheath
 331 boundary layer, while, over the same range of α s, the open circles correspond to bow
 332 shock associated turbulent intervals.

333 The horizontal lines in Figure 5 show that, over the turbulence range, the average of
 334 $\langle b_X^2 \rangle$ and $\langle b_Z^2 \rangle$ is larger while the average of $\langle b_Y^2 \rangle$ is smaller than over the
 335 noise range of scaling indices. Therefore, when turbulence is observed $\langle b_X^2 \rangle$ dominates
 336 over $\langle b_Y^2 \rangle$ and the latter is still stronger than the increased $\langle b_Z^2 \rangle$. Magnetosheath
 337 boundary layer associated turbulence intervals (filled circles - intervals **c** in Figure 2) show

338 even larger $\langle b_X^2 \rangle$ values than the near-shock turbulence values (open circles - intervals **e**
339 in Figure 2, over the same α range). In accordance with our findings, the analysis of PVO
340 magnetic, electric and plasma data has shown that, near the terminator region but within
341 the magnetosheath boundary layer, the magnetic field is nearly aligned with the Sun-Venus
342 line (X VSO direction). It was interpreted in terms of a friction-like viscous interaction
343 between the shocked solar wind and the ionospheric plasma over the magnetic polar regions
344 where the draped interplanetary magnetic field lines slip over the planet (Perez-de-Tejada
345 et al., 1993). The viscous plasma-plasma interaction and frictional heating can explain
346 the enhanced temperatures inside the magnetosheath boundary layer, observed tailward
347 by Venera 10 (Romanov et al. 1978). An alternative explanation is represented by local
348 turbulent heating of the boundary layer plasma. We note that near the magnetopause,
349 where VEX crosses the turbulent boundary layer, the draped interplanetary magnetic
350 field lines are more stretched having a large X VSO component (Figure 4). Although
351 the number of events is rather limited, the near-shock turbulent regions have smaller
352 X VSO but larger perpendicular Y VSO and Z VSO magnetic components than the
353 magnetosheath boundary layer turbulence (Figure 5).

354 Finally, noise (open circles - intervals **d** in Figure 2) is associated with a large $\langle b_Y^2 \rangle$,
355 smaller $\langle b_X^2 \rangle$ and almost negligible $\langle b_Z^2 \rangle$. Since the IMF is mostly in the X-Y
356 plane, the large-scale magnetosheath magnetic field is not affected by the boundaries, but
357 exhibiting only noisy broad-band fluctuations and it has the strongest average components
358 in the X-Y plane.

359 Let us investigate deeper now the intermittent nature of turbulence. Besides the char-
360 acteristic scaling exponents ($\alpha \sim 1.6$) and the expected average magnetic field directions,

361 intermittency represents another key feature of fully developed turbulence. Therefore, the
 362 occurrence of intermittency represents a further evidence that we are dealing with a real
 363 turbulence, capable of heating the background plasma.

4.2. Turbulent intermittency versus Gaussianly distributed noise

364 Higher order statistics is needed to fully describe the nature of nonlinear fluctuations. In
 365 turbulent, non-homogeneous plasma flows the shape of the probability density functions
 366 (PDFs) is scale-dependent and peaked with long tails (e.g. Frisch, 1995). Because of the
 367 shortness of time series during one crossing the shapes of non-Gaussian PDFs or their
 368 scale dependency cannot be evaluated (Vörös et al., 2008). Instead, we construct PDFs
 369 from the 15 magnetic time series (realizations) of turbulence for which spectral scaling
 370 near $\alpha \sim 1.6$ was observed (events from both **c** and **e** intervals in Figure 2). Splitting
 371 the data into magnetosheath boundary layer and near-shock turbulence regions would
 372 not change the shape of turbulent PDFs significantly. PDFs corresponding to the noisy
 373 magnetosheath (intervals **d** in Figure 2) will be also reconstructed.

374 PDFs of two-point differences of magnetic field strength were estimated from $\delta B =$
 375 $B(t + \tau) - B(t)$, for $\tau = 2 \dots 30$ s. Figure 6 shows the PDFs for $\tau = 3, 30$ s only. Boundary
 376 turbulence associated PDFs are shown on the left, 1/f noise related PDFs on the right
 377 hand side. The error bars represent 95% confidence limits for the mean in each point of δB .
 378 The dashed grey points are least-square Gaussian fits to the experimental two-point PDFs.
 379 The Gaussian PDF is given by $\frac{1}{\sigma\sqrt{2\pi}} \exp(-\frac{(x-\mu)^2}{2\sigma^2})$, where μ is the mean and σ^2 is the
 380 variance. For the smaller time scale $\tau = 3$ s the tails of the experimental turbulent PDFs
 381 are higher than the Gaussian tails. The departure from the Gaussian indicates that non-
 382 homogeneously distributed fluctuations become more probable as the scale decreases due

383 to turbulent structures and long-range interactions (Leubner and Vörös, 2005). Gradual
 384 decorrelation is obtained by enhancing the two-point separation scale and a Gaussian
 385 is approached for large enough τ even in a turbulent field. This is because the typical
 386 correlations for turbulent structures are lost if the separation is large, and only Gaussianly
 387 distributed noise is observed. For $\tau = 30$ s, the PDF is a Gaussian in Figure 6 left. Noise
 388 shows Gaussianly distributed PDFs over both time scales.

Let us further investigate the shape of PDFs in terms of statistical moments. Using standard procedures (Press et al., 1992), the skewness (S) or the third moment,

$$S(\tau) = \frac{1}{N} \sum_{j=1}^N \left(\frac{x_j - \bar{x}}{\sigma} \right)^3 \quad (1)$$

and the kurtosis (K) or the fourth moment,

$$K(\tau) = \frac{1}{N} \sum_{j=1}^N \left(\frac{x_j - \bar{x}}{\sigma} \right)^4 - 3 \quad (2)$$

389 are computed for turbulent and noisy intervals, as above. Here $x_j = \delta B(t_j, \tau)$, σ is the
 390 standard deviation, \bar{x} is the mean value of the elements and N is the number of the data
 391 points. In this way the dimensionless $S(\tau)$ and $K(\tau)$ characterize the scale and time
 392 evolution of the shape of a distribution (S - asymmetry around the mean; K - peakedness
 393 or flatness; both relative to a Gaussian distribution, for which $S = K = 0$). K increases
 394 towards small scales in intermittent turbulence (Frisch, 1995).

395 Figure 7 shows the time-scale (τ) evolution of kurtosis $K(\tau)$ (top) and skewness $S(\tau)$
 396 (bottom) for turbulent (left) and noisy (right) intervals. The error bars represent 95%
 397 confidence limits for the mean in each value of τ . As is expected from turbulent PDFs
 398 in Figure 6, K is increasing as τ decreases, which proves that the underlying magnetic

399 fluctuations are non-Gaussian, peaked and intermittent. K practically does not depend
400 on τ in the case of $1/f$ noise, indicating a Gaussianly distributed process.

401 The skewness remains close to zero (Figure 7: bottom) in both cases, showing symmetric
402 distributions around the mean value.

5. Discussion and conclusions

403 In this paper the unique data from the VEX spacecraft were used to investigate magnetic
404 fluctuation statistics from Venusian magnetosheath and wake regions. The interaction of
405 the solar wind with the planet drives magnetic fluctuations exhibiting different scaling
406 regimes in different regions of near-Venusian space. To identify spectral scaling ranges
407 and indices, we used a wavelet technique, successfully applied for studying the continuous
408 spectra in the Earth's plasma sheet turbulence (Vörös et al., 2004). The technique and
409 the data intervals were not optimized for finding waves (peaks in power spectra).

410 Three types of scaling were observed. Inside the dayside/tailward magnetosheath, far
411 from boundaries, $1/f$ noise is present in the prevailing majority of cases indicating the
412 contribution of multiple independent driving sources. It also means, that this type of
413 spectral scaling is not formed by an isolated single physical process. In other words, there
414 might exist multiple sources of fluctuations, but no one of them is close enough in space
415 to dominate in the spectral power. This changes when VEX enters to a region where
416 multiple sources are missing, or where a single physical process dominates with a scaling
417 feature other than that of the noise. In fact, these are distinct regions of near -Venusian
418 space where the 'solar wind - planetary obstacle' interactions are enhanced or the multiple
419 sources of noise are shielded.

420 The interaction is enhanced at the terminator ionopause, probably due to the Kelvin-
421 Helmholtz instability, at the magnetosheath boundary layer due to the magnetosheath
422 boundary shear flows and near the quasi-parallel bow-shock. The near-planet wake rep-
423 resents a region which is shielded from the plasma of solar wind origin. Filamentary
424 structures, detached plasma clouds, depleted density holes and radially aligned draped
425 magnetic field lines were observed by PVO spacecraft in the near-planet night side wake
426 (Luhmann and Russel, 1983; Marubashi et al., 1985). The magnetosheath flow is expected
427 to converge into the wake only near $5 R_V$ behind the planet (Intriligator et al., 1979). The
428 observed wavy structures near the terminator and in the night side near-planet wake can
429 be associated with the detached coherent structures or holes. The occurrence/absence of
430 these structures can be controlled by the direct interaction between the solar wind and
431 ionosphere, e.g. by the high/low solar wind dynamic pressure. In our interpretation, the
432 spectral index $\alpha \sim 2.5$ indicates, that the coherent wavy structures represent the domi-
433 nating physical process in this region. Because of the shielding of the near planet wake,
434 turbulence or noise are absent in this region. Due to the converging flows the shielding
435 can disappear at distances close to or larger than $X VSO \sim 5R_V$, where the character of
436 fluctuations would change.

437 The magnetosheath regions with distinct scaling indices (turbulence or noise) partially
438 overlap (see Figure 2). This can be explained through a movement of boundaries under
439 the influence of changing upstream IMF conditions. Spatial intermittency, typical for
440 turbulence with scale-dependent non-Gaussian distributions, can lead also to interwoven
441 scaling structures. The turbulent regions are formed near the 'supersonic solar wind flow
442 - planetary obstacle' boundaries in the presence of draped IMF. The outer boundary is

443 the bow shock, where the solar wind slows down and heated for the first time. Here, the
444 local turbulence is associated with the quasi-parallel shock geometry. Second time the
445 solar wind flow decelerates at the inner magnetosheath producing a velocity shear near
446 the magnetosheath boundary layer. The near-terminator ionosphere/magnetopause and
447 its interaction with the solar wind plays an important role. The rarefaction wave (the
448 boundary) and the observed plasma conditions in the tailward boundary layer can emerge
449 from the magnetopause near the terminator and extend downstream (Perez-de-Tejada et
450 al., 1991). Local heating of the plasma within the boundary layers is also possible through
451 the shear flow associated turbulence. The spatial size of boundary layer turbulence (see
452 Figure 2) is roughly between 0.5 and 1 R_V , shorter turbulent intervals were observed
453 near the quasi-parallel bow shock. The width of the noisy magnetosheath in between
454 the turbulent boundaries is of the same order. The estimation of the spatial sizes of
455 these regions is rather rough. The data are available only from single point measurements
456 (the boundaries can move during the measurements) and the 12 min long data intervals
457 represent a pure resolution. The estimation of scaling indices within shorter time intervals,
458 however, was not possible due to the large statistical errors in these cases. Multi-point
459 Cluster observations show, that turbulence downstream of the quasi-parallel terrestrial
460 bow shock is intermittent and that the level of intermittency increases over the spacecraft
461 separation, reaching larger values than 8000 km (Yordanova et al., 2008). Our results
462 show, that the spatial scale of intermittent turbulence is less than 1 R_V near the Venusian
463 bow shock. In between the near shock region and the magnetosheath boundary layer
464 fluctuations are noisy (in Figure 4, squares between triangles).

465 It was shown by Perez-de-Tejada et al. (1993) that the magnetic field is nearly aligned
466 with the Sun-Venus line (X VSO direction) within the near-terminator magnetosheath
467 boundary layer. We found a similar alignment within the boundary layer at a distance of
468 $X_{VSO} \sim -2.2R_V$ (Figures 2, 5). It indicates, that the magnetic field geometry detected
469 during the viscous plasma-plasma interactions near the terminator ionosphere is conserved
470 and observed further downstream along the VEX trajectory, where the draped magnetic
471 field is stretched (Figure 4).

472 Data intervals that were found to be turbulent or noisy in the spectral analysis were fur-
473 ther investigated using the two-point (time delayed) probability density functions (PDFs).
474 Over large two-point separations (e.g. $\tau = 30s$), both turbulent and noisy PDFs are well
475 fitted by the Gaussian distributions, indicating the occurrence of uncorrelated fluctuations.
476 Over small separations (e.g. $\tau = 3s$), large deviations from the Gaussian distribution are
477 observed only for turbulent intervals, noise remains Gaussianly distributed (Figure 6).
478 The scale -dependency of kurtosis (Figure 7) shows that turbulent structures are inter-
479 mittently distributed, noise is more homogeneous. Skewness remains close to zero in
480 both cases which corresponds to symmetrical distributions. A simultaneous increase of S
481 and K towards small scales would indicate that the multi-scale fluctuations in turbulence
482 might be affected by strong large -scale gradients or close boundaries (Vörös et al., 2007).
483 Therefore, $S(\tau) \sim 0$ for $\tau \in (2 - 30)$ s is a signature of intermittency, not affected by
484 boundaries along the VEX trajectory over the scale of seconds. However, asymmetries or
485 nonzero skewness in magnetic field statistics can appear below the 1 s time scale. Anyhow,
486 besides the expected spectral index ($\alpha \sim 1.6$), the observation of intermittency represents
487 a further evidence for the occurrence of real turbulence in the near-Venusian space. The

488 key feature of turbulence is its strong dissipative nature and a capability for the local
489 heating of plasma. Multi-scale turbulence can channel the large-scale energy of the flow
490 to kinetic scales, where dissipation processes are strong. We will investigate this point in
491 a different paper.

492 **Acknowledgments.** The work of Z.V. and M.P.L. was supported by the Austrian
493 Wissenschaftsfonds under grant number P20131-N16.

References

- 494 Abry, P., P. Flandrin, M. S. Taqqu, and D. Veitch (2000), Wavelets for the analysis, esti-
495 mation and synthesis of scaling data, in Self-Similar Network Traffic and Performance
496 Evaluation, edited by K. Park and W. Willinger, p. 39, Wiley-Interscience.
- 497 Amerstorfer, U.V., N.V. Erkaev, D. Langmayr, and H.K. Biernat (2007), On Kelvin-
498 Helmholtz instability due to the solar wind interaction with unmagnetized planets,
499 *Planet. Space Sci.*, *55*, 1811–1816, doi:10.1016/j.pss.2007.01.015.
- 500 Balikhin, M.A., S. A. Pope, T. L. Zhang, A.O. Fedorov, M. Gedalin, and S. Barabash
501 (2008), Giant Vortices Lead to Ion Escape From Venus, submitted to *Geophys.Res.*
502 *Lett.*.
- 503 Bauer, S.J., L.H. Brace, D.M. Hunten, D.S. Intriligator, W.C. Knudsen, A.F. Nagy, C.T.
504 Russell, F.L. Scarf, and J. H. Wolfe (1977), The Venus ionosphere and solar wind
505 interaction, *Space Sci. Rev.*, *20*, 413–430.
- 506 Biernat, H.K., N.V. Erkaev, U.V. Amerstorfer, T. Penz, and H.I.M. Lichtenegger (2007),
507 Solar wind flow past Venus and its implications for the occurrence of the Kelvin-
508 Helmholtz instability, *Planet. Space Sci.*, *55*, 1793–1803, doi:10.1016/j.pss.2007.01.015.

- 509 Brace, L. H., R.F. Theis, and W.R. Hoegy (1982), Plasma clouds above the ionopause of
510 Venus and their implications, *Planet. Space Sci.*, *30*, 29-37.
- 511 Bridge, H.S., A.J. Lazarus, C.W. Snyder, E.J. Smith, L. Jr. Davis, P.J.Jr. Coleman, and
512 D.E. Jones (1967), Mariner V: Plasma and magnetic fields observed near Venus, *Science*,
513 *158*, 1669–1673.
- 514 Elphic, R.C., C.T. Russel, J.G. Luhmann, F.L. Scarf, and L.H. Brace (1981), The Venus
515 ionopause current sheet: thickness, length, scale and controlling factors, *J. Geophys.*
516 *Res.*, *86*, 11430–11438.
- 517 Frisch, U. (1995), *Turbulence, the legacy of A.N. Kolmogorov*, Cambridge University
518 Press.
- 519 Intriligator, D.S., H.R. Collard, J.D. Mihalov, R.C. Whitten, and J.H. Wolfe (1979),
520 Electron observations and ion flow from the Pioneer Venus Orbiter Plasma Analyzer
521 Experiment, *Science*, *205*, 116–119.
- 522 Leubner, M. P. and Vörös, Z. (2005), A nonextensive entropy approach to solar wind
523 intermittency, *Astrophys. J.*, *618*, 547–555.
- 524 Luhmann, J. G., and C.T. Russell (1983), Magnetic fields in the ionospheric holes of
525 Venus: evidence for an intrinsic field? , *Geophys. Res. Lett.*, *10*, 409–412.
- 526 Luhmann, J. G., C. T. Russell, K. Schwingenschuh, and Y. Yeroshenko (1991), A compar-
527 ison of induced magnetotails of planetary bodies: Venus, Mars and Titan, *J. Geophys.*
528 *Res.*, *96*, 11199–11208.
- 529 Luhmann, J.G., M. Tatrallyay, C. T. Russell, and D. Winterhalter (1983), Magnetic field
530 fluctuations in the Venus magnetosheath, *Geophys. Res. Lett.*, *10*, 655–658.

- 531 Marubashi, K., J.M. Grebowsky, H.A. Taylor, J.G. Luhmann, C.T. Russel, and A. Barnes
532 (1985) Ionosheath plasma flow in the wake of Venus and the formation of ionospheric
533 holes, *J. Geophys. Res.*, *90*, 1385–1398.
- 534 Pérez-de-Tejada, H., D.S. Intriligator, and R.J. Strangeway (1991), Steady-state plasma
535 transition in the Venus ionosheath, *Geophys. Res. Lett.*, *18*), 131–134.
- 536 Pérez-de-Tejada, H., D.S. Intriligator, and R.J. Strangeway (1993), Magnetic field prop-
537 erties of the intermediate transition of the Venus ionosheath, *Geophys. Res. Lett.*, *20*),
538 991–994.
- 539 Press, W.H., B.P. Flannery, S.A. Teukolsky, and W.T. Vetterling (1992), Numerical
540 recipes in C: The art of scientific computing, Cambridge University Press.
- 541 Romanov, S., V. Smirnov, and O. Vaisberg (1978), Interaction of the solar wind with
542 Venus, *Kosmich. Issled.*, *16*), 746.
- 543 Russell, C.T. (1992), The Pioneer Venus mission, in. Venus and Mars: Atmospheres,
544 Ionospheres and Solar Wind Interactions, *AGU Geophys Monogr. Series*, *66*, (eds. J.
545 G. Luhmann, M. Tatrallyay, and R. O. Repin), 225–236.
- 546 Russell, C.T., and O. Vaisberg (1983), The interaction of the solar wind with Venus,
547 *Venus*, (eds. D.M. Hunton, L Colin, T.M. Donahue, V.I. Moroz), 873–940.
- 548 Spreiter, J. R., and S.S. Stahara (1992), Computer modeling of solar wind interaction
549 with Venus and Mars, in. Venus and Mars: Atmospheres, Ionospheres and Solar Wind
550 Interactions, *AGU Geophys Monogr. Series*, *66*, (eds. J. G. Luhmann, M. Tatrallyay,
551 and R. O. Repin), 345–383.
- 552 Terada, N., S. Machida, and H. Shinagawa (2002), Global hybrid simulation of the
553 Kelvin-Helmholtz instability at the Venus ionopause, *J. Geophys. Res.*, *107*(A12), 1471,

554 doi:10.1029/2001JA009224.

555 Volwerk, M., T.L. Zhang, M. Delva, Z. Vörös, W. Baumjohann and K.-H. Glassmeier
556 (2008a), First identification of mirror mode waves in Venus' magnetosheath? *Geophys.*
557 *Res. Lett.*, *35*, L12204, doi:10.1029/2008GL033621.

558 Volwerk, M., T.L. Zhang, M. Delva, Z. Vörös, W. Baumjohann and K.-H. Glassmeier
559 (2008b), A statistical study of mirror mode like structures in Venus' magnetosheath,
560 submitted to *J. Geophys. Res.*.

561 Vörös, Z. et al.(2004), Magnetic turbulence in the plasma sheet, *J. Geophys. Res.*, *109*,
562 A11215, doi:10.1029/2004JA010404.

563 Vörös, Z., W. Baumjohann, R. Nakamura, A. Runov, M. Volwerk, T. Takada, E. A.
564 Lucek, and H. Rème (2007), Spatial structure of plasma flow associated turbulence in
565 the Earths plasma sheet, *Ann. Geophys.*, *25*, 13–17.

566 Vörös, Z., T.L. Zhang, M. P. Leubner, M. Volwerk, M. Delva, W. Baumjohann and K.
567 Kudela (2008), Magnetic fluctuations and turbulence in the Venus magnetosheath and
568 wake, *Geophys. Res. Lett.*, *35*, L11102, doi:10.1029/2008GL033879.

569 Wolff, R., B. Goldstein, and C. Yeates (1980), The Onset and Development of Kelvin-
570 Helmholtz Instability at the Venus Ionopause, *J. Geophys. Res.*, *85(A13)*, 7697-7707.

571 Yordanova, E., A. Vaivads, M. Andr, S.C. Buchert, and Z. Vörös (2008), Magnetosheath
572 plasma turbulence and its spatiotemporal evolution as observed by the Cluster space-
573 craft *Phys.Rev.Lett.*, *100*, 205003-1–205003-4.

574 Zhang Z.L., et al. (2006), Magnetic field investigation of the Venus plasma environment:
575 Expected new results from Venus Express, *Planet.Space Sci.*, *54*, 1336–1343.

576 Zhang T.L., et al. (2007), Little or no solar wind enters Venus atmosphere at solar mini-
577 mum, *Nature*, 450, 654–656, doi:10.1038/nature06026.

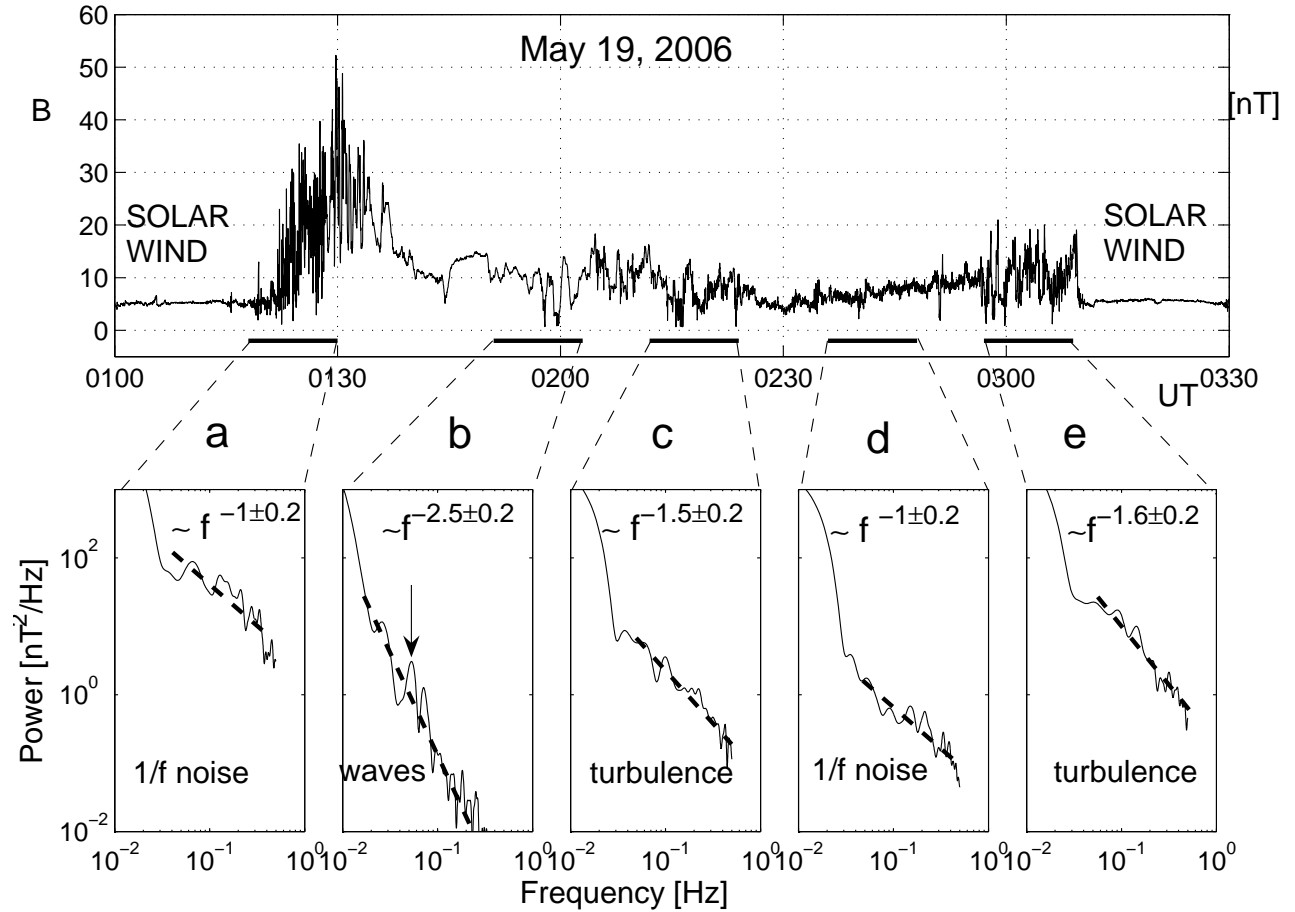


Figure 1. Top: Magnetic field strength (B) on May 19, 2006. The horizontal black lines correspond to the time intervals **a** - **e** of equal length in the dayside magnetosheath (**a**), night side near-planet wake (**b**), magnetosheath boundary layer (**c**), tailward magnetosheath (**d**), and in the vicinity of the bow shock; Bottom: Power spectra and spectral scalings estimated within the intervals **a** - **e**. Pronounced wavy structures are present mainly in the wake (interval **b**). The vertical arrow points to the spectral peak at ~ 15 s.

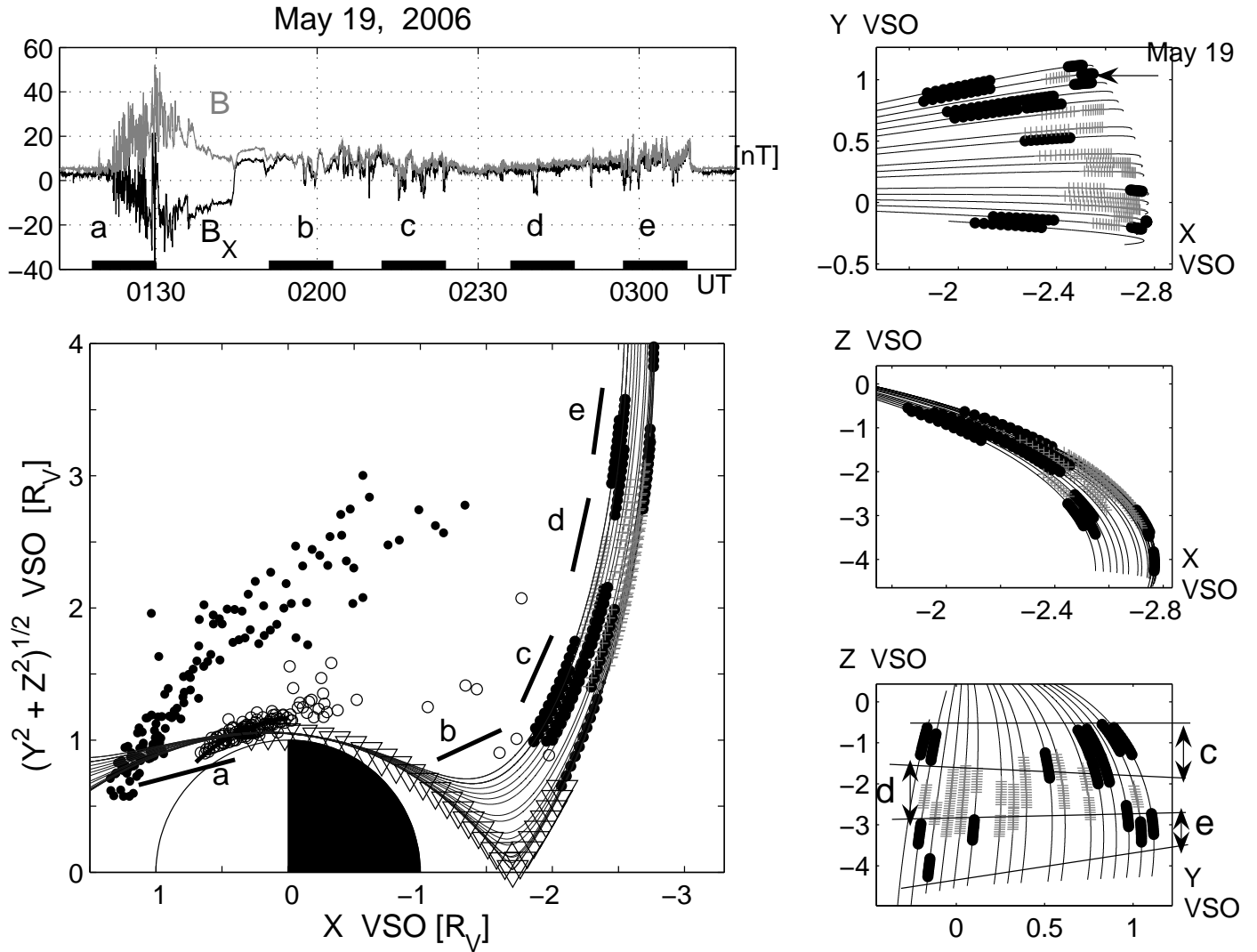


Figure 2. Top left: Magnetic field strength (B, grey line) and B_X magnetic component (black line) on May 19, 2006; the horizontal lines show the intervals **a-e** depicted in Figure 1; Bottom left: VEX crossings (thin black lines) of the Venusian plasma environment in VSO coordinates. The intervals **a-e** (black lines) are shown alongside the VEX trajectories. The filled circles show the bow shock, the open circles show the magnetopause during multiple crossings (after Zhang et al., 2007). The large triangles along the lowest trajectory correspond to the region of wavy structures and spectral scaling index $\alpha \sim 2.5$. The family of thick black lines along the trajectories (intervals **c** and **e**) correspond to turbulent regions with $\alpha \sim 1.6$. The grey '+' signs are intervals of $1/f$ noise (interval

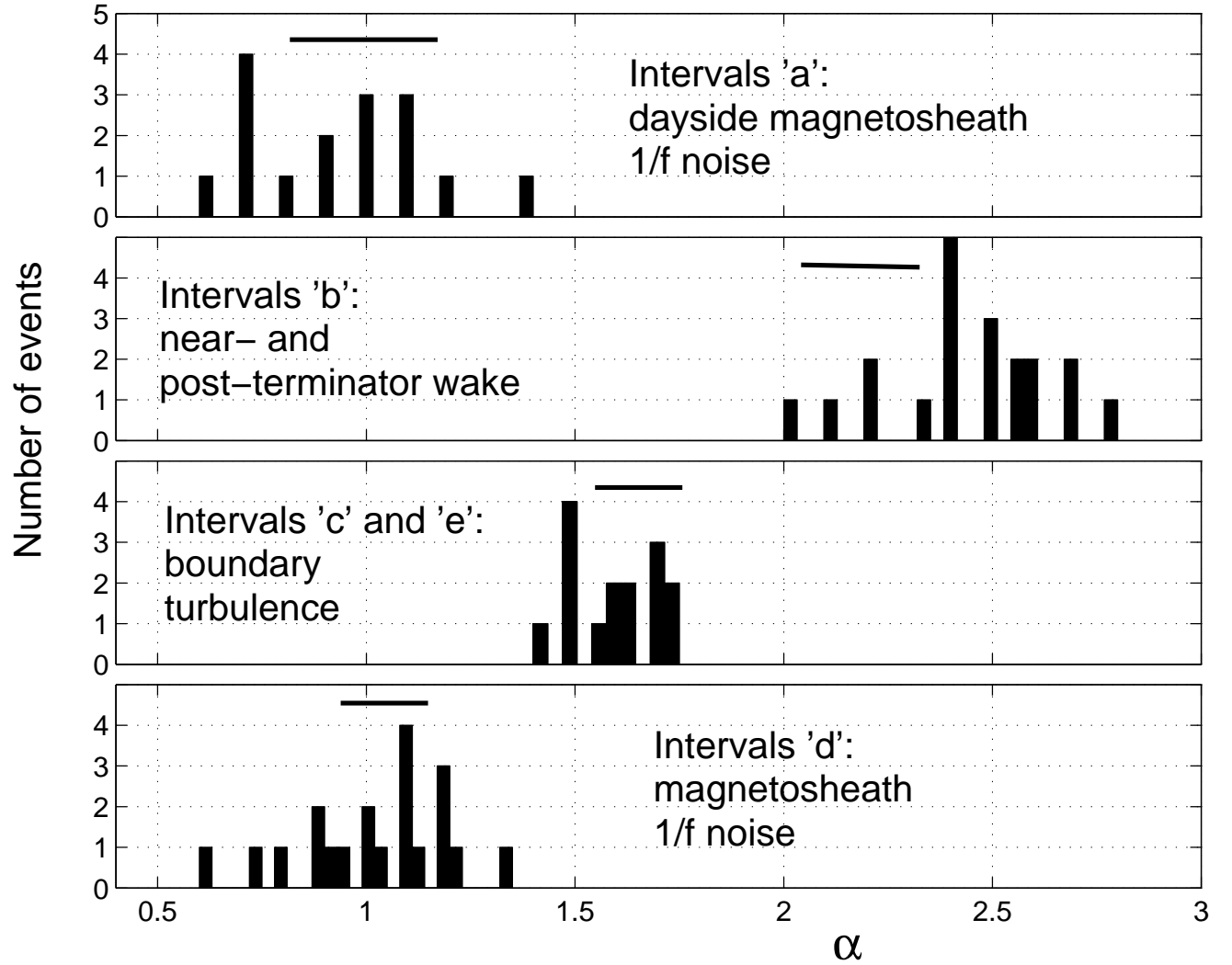


Figure 3. Histograms of the scaling indices in different regions of near-Venusian space (approximately obtained during the intervals **a-e** in Figure 2.). From top to bottom: dayside magnetosheath (**a**); near and post-terminator wake (**b**); magnetosheath boundary and near bow shock region (**c-e**); post-terminator tailward magnetosheath (**d**). These spatial regions are depicted more clearly in Figure 4.

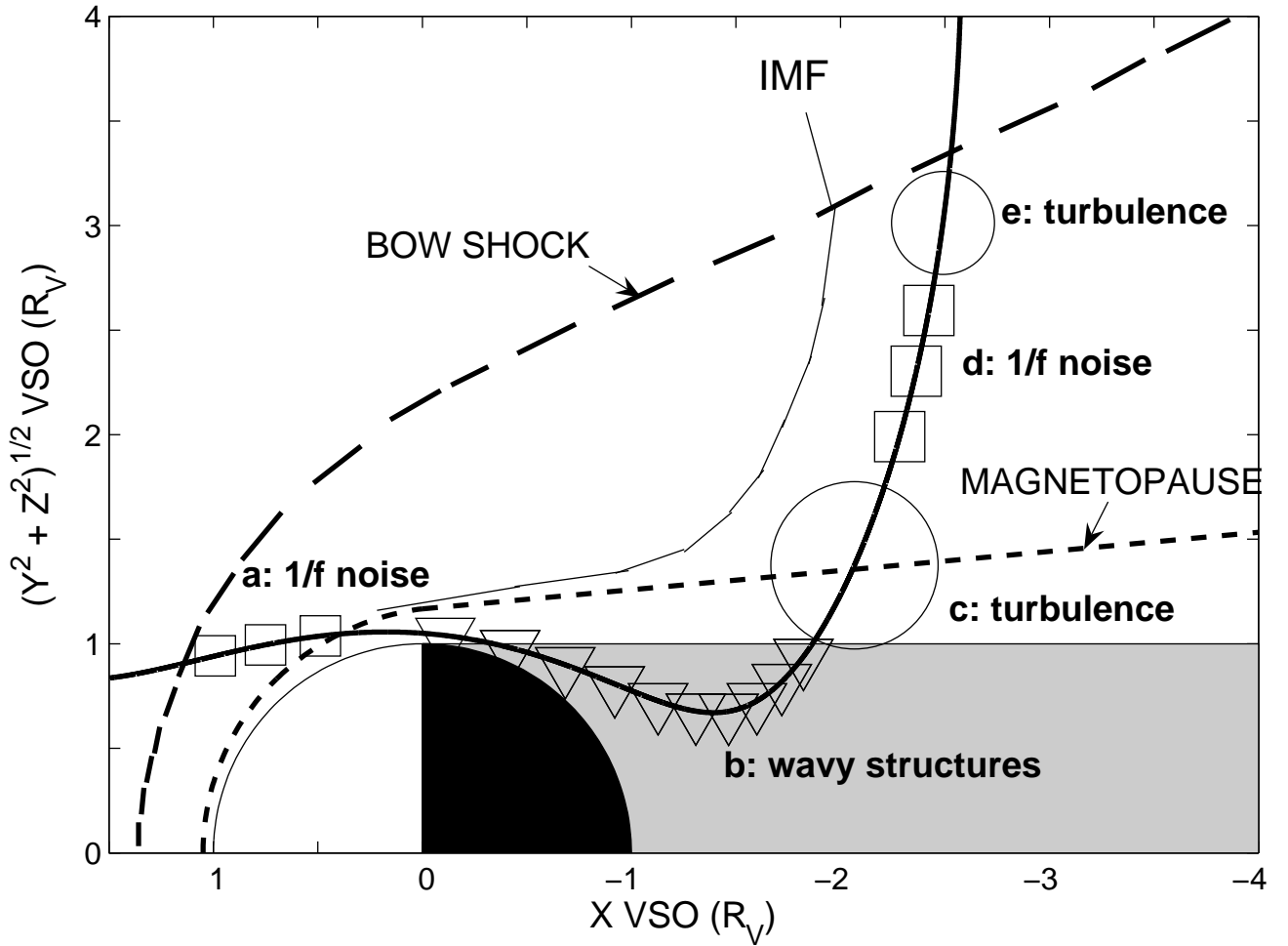


Figure 4. A cartoon showing the type of physical processes in the spatial regions of near-Venusian space; the magnetopause and the bow shock (dashed lines); a VEX crossing (solid black line); the optical shadow (shaded region); draped IMF (thin black line); the time intervals/spatial regions **a-e** are marked with squares, triangles, circle, squares, and circle, respectively.

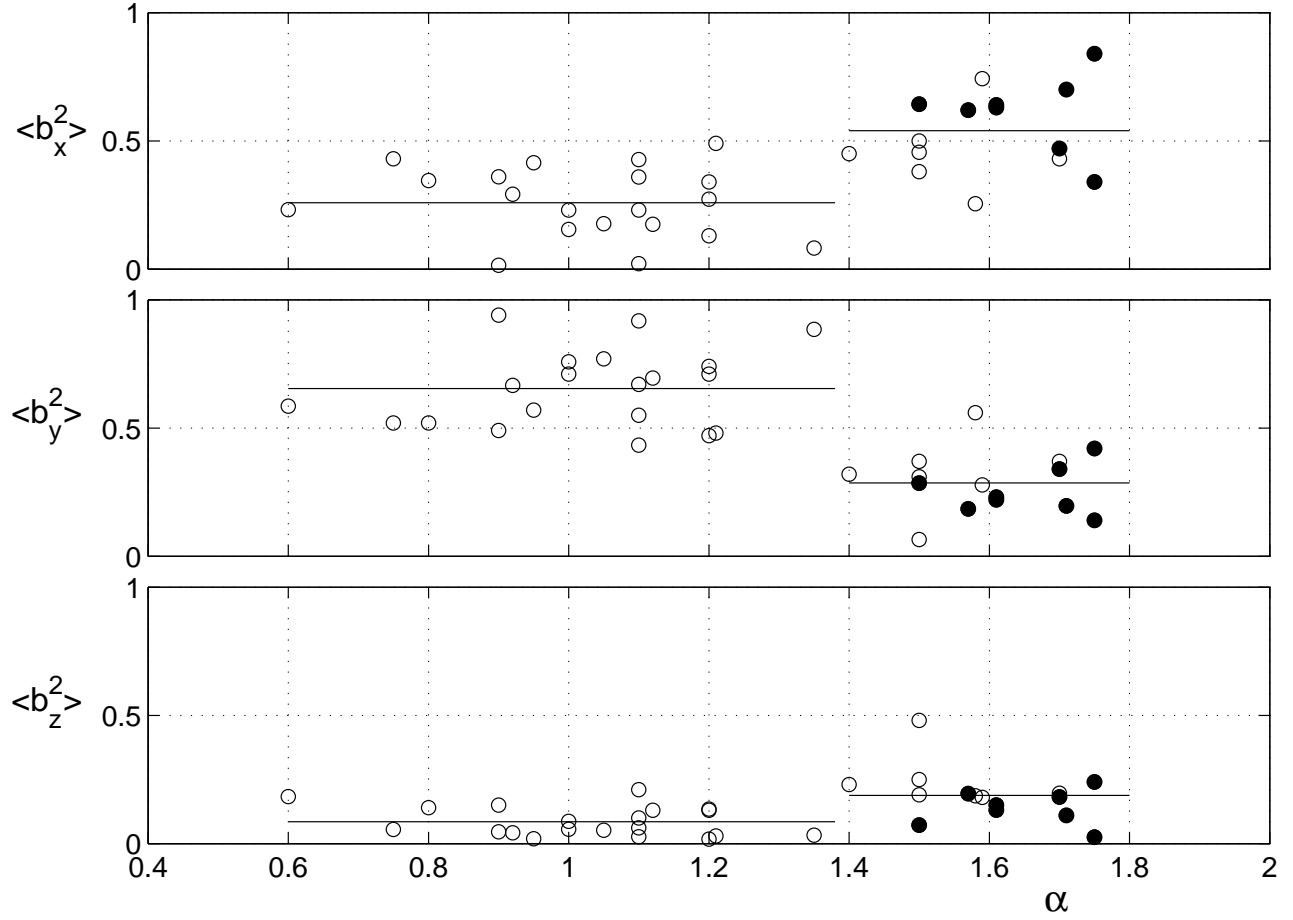


Figure 5. From top to bottom: comparison of 12 min averages of $\langle b_X^2 \rangle$, $\langle b_Y^2 \rangle$ and $\langle b_Z^2 \rangle$ with the observed spectral scaling indices α ; The subscripts indicate VSO magnetic field components; The horizontal lines correspond to averages of points (open and filled circles) over the noisy $\alpha \in (0.6 - 1.4)$ and turbulent $\alpha = 1.6 \pm 0.2$ scaling index ranges in each subplot; The turbulent intervals include boundary layer (filled circles) and near-shock (open circles) events; For each 12 min interval $b_X^2(t) + b_Y^2(t) + b_Z^2(t) = 1$.

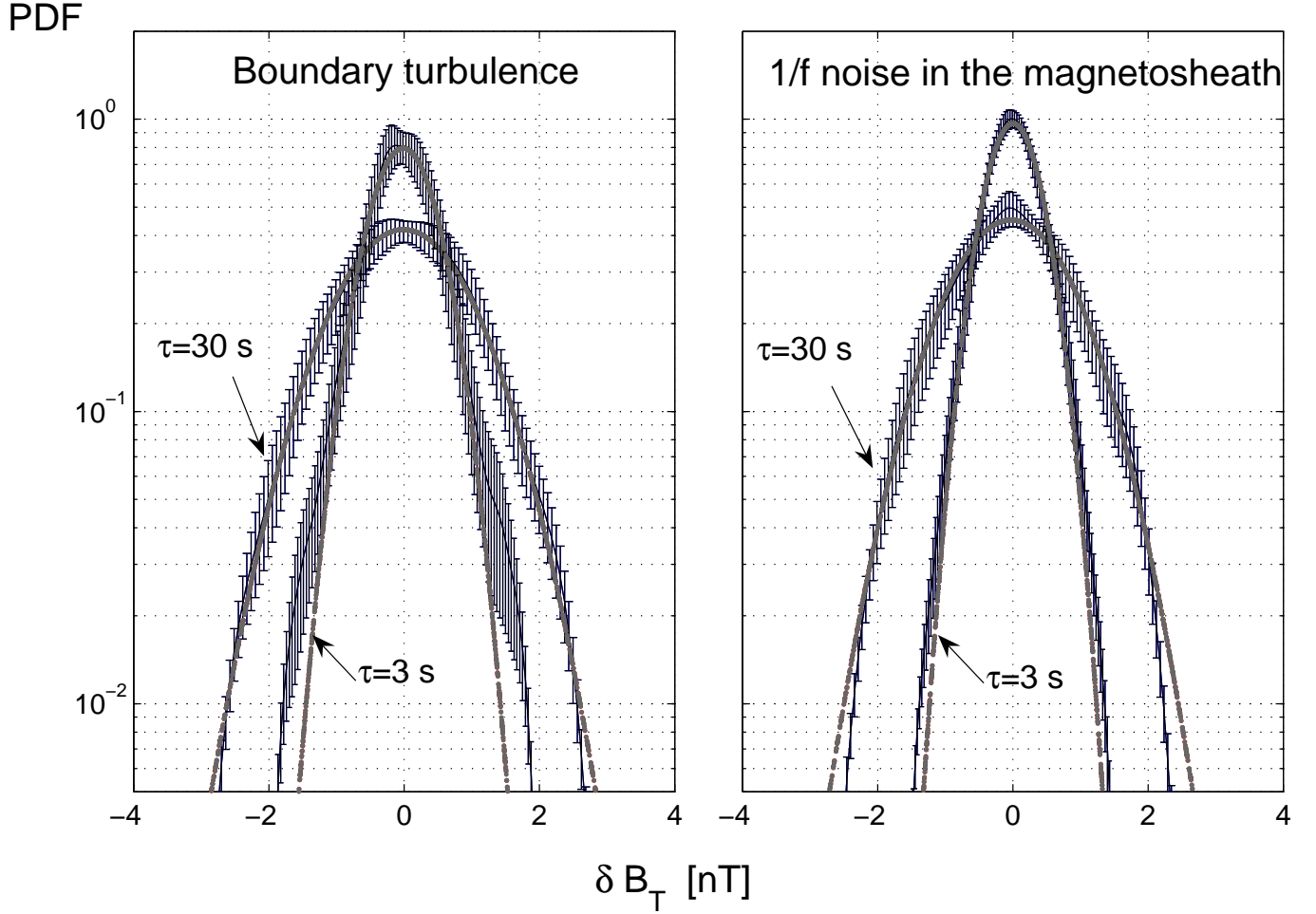


Figure 6. Probability density functions (PDFs) constructed from magnetic time series (two-point differences defined through $\delta B = B(t + \tau) - B(t)$) of turbulent (left) and noisy (right) intervals. Gaussian fits are shown as dashed grey lines. At small scales (e.g. $\tau = 3$ s) the PDF is a non-Gaussian for turbulent time series and Gaussian for noisy time series. At large scales (e.g. $\tau = 30$ s) the PDF is a Gaussian in both cases. The error bars represent 95% confidence limits for the mean in each point of δB_T .

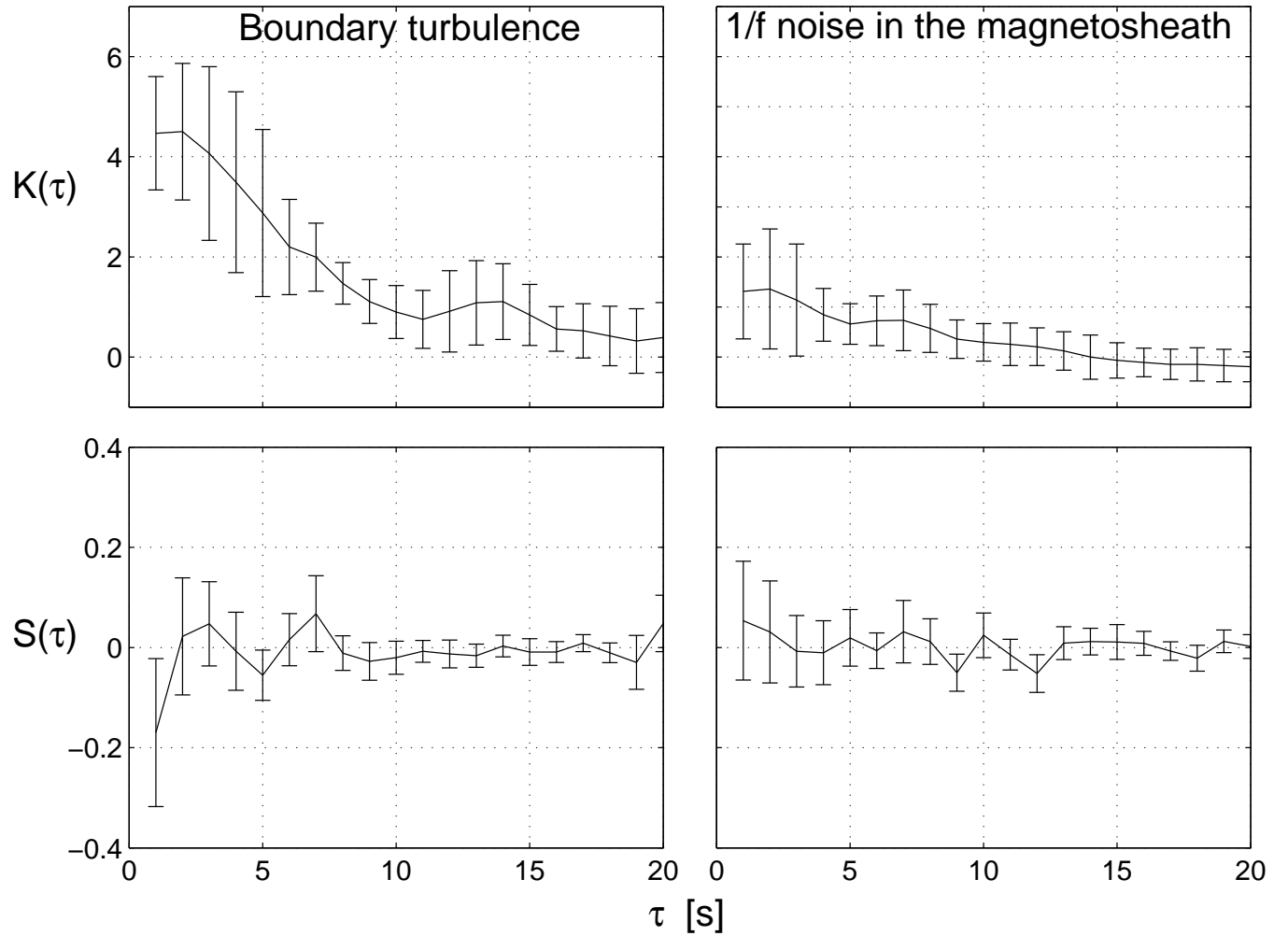


Figure 7. The evolution of kurtosis (K , top) and skewness (S , bottom) with the time scale τ , computed from two-point differences defined through $\delta B = B(t + \tau) - B(t)$ of turbulent (left) and noisy (right) time intervals. K - peakedness of the PDF; S - asymmetry around the mean, both relative to a Gaussian distribution, for which $S = K = 0$; The error bars represent 95% confidence limits for the mean in each value of τ .